

Molecular simulation of the surface tension of 33 multi-site models for real fluids

Stephan Werth^a, Martin Horsch^{a,*}, Hans Hasse^a

^a*University of Kaiserslautern, Laboratory of Engineering Thermodynamics, Erwin-Schrödinger Str. 44, 67663 Kaiserslautern, Germany*

Abstract

Molecular models of real fluids are validated by comparing the vapour-liquid surface tension from molecular dynamics (MD) simulation to correlations of experimental data. The considered molecular models consist of up to 28 interaction sites, including Lennard-Jones sites, point charges, dipoles, and quadrupoles. They represent 33 real fluids, such as ethylene oxide, sulfur dioxide, phosgene, benzene, ammonia, formaldehyde, methanol, and water, and were adjusted to reproduce the saturated liquid density, the vapour pressure, and the enthalpy of vaporization. The models were not adjusted to interfacial properties, however, so that the present MD simulations are a test of model predictions. It is found that all of the considered models overestimate the surface tension. In most cases, however, the relative deviation between the simulation results and correlations to experimental data is smaller than 20 %. This observation corroborates the outcome of previous studies on the surface tension of two-centre Lennard-Jones plus point quadrupole (2CLJQ) and two-centre Lennard-Jones plus point dipole (2CLJD) fluid models, where an overestimation of the order of 10 to 20 % was found.

Keywords: Molecular simulation, surface tension, vapour-liquid equilibrium

1. Introduction

Interfacial properties are important for many applications in process engineering, including processes like absorption, wetting, nucleation, cavitation, and foaming. Experimental data on the surface tension are available for pure fluids, but the temperature range is usually limited to ambient conditions [1, 2]. Hence, it is desirable to have models which allow predicting interfacial properties of pure fluids and mixtures over a wide temperature and pressure range. Molecular modelling and simulation can be used for this purpose if the underlying force fields are accurate [3].

Molecular models for many low-molecular fluids were developed in previous work of our group [4–15] and recent work by Vrabec and co-workers [11–21]. The molecular model parameters were adjusted to describe the saturated liquid density, the vapour pressure, and the enthalpy of vaporization, which they do well. These models were also used to predict transport properties, yielding good results for the shear viscosity, the thermal conductivity, and self-diffusion coefficients of pure fluids [15, 16, 20–22] and mixtures [22–26]. Several fluid models discussed in the present work have recently been used to develop fundamental equations of state based on molecular simulation as well as experimental data, i.e. the models for ethylene oxide [27], phosgene [28], hexamethyldisiloxane [20], and octamethylcyclotetrasiloxane [21]. The surface tension was not part of the parameterization and is thus strictly predictive.

In previous work, systematic evaluations of the surface tension of the two-centre Lennard-Jones plus point quadrupole (2CLJQ) and the two-centre Lennard-Jones plus point dipole (2CLJD) molecular model classes were conducted [29, 30]. These models, on average, overestimate the surface tension by about 20 %

*Corresponding author. E-mail: martin.horsch@mv.uni-kl.de; phone: +49 631 205 3227; fax: +49 631 205 3835.

and 12 %, respectively [30, 31]. Other molecular models which have been adjusted to bulk properties, but not to interfacial properties, exhibit similar deviations [32–40].

In the present work, the existing multi-site models are used as they are. No parameters are changed. By molecular dynamics (MD) simulation, predictions of interfacial properties from bulk properties are obtained. Used in this way, molecular modelling can be compared to other approaches for predicting the surface tension from bulk data, such as phenomenological parachor correlations [41–44], corresponding-states or critical-scaling expressions [44, 45], which are also phenomenological correlations, and other molecular methods, e.g. square gradient theory [46] and density functional theory [47, 48] on the basis of molecular equations of state [49–52].

In the present work, bulk and interfacial properties of real fluids are determined simultaneously from heterogeneous MD simulations. The simulation results are compared with correlations to experimental data, where available.

2. Molecular simulation

The molecular models discussed in the present work [4–21] are internally rigid and consist of Lennard-Jones (LJ) sites with superimposed electrostatics. The total potential energy is given by

$$\begin{aligned}
U = & \sum_{i=1}^{N-1} \sum_{j=i+1}^N \left(\sum_{a=1}^{n_i^{\text{LJ}}} \sum_{b=1}^{n_j^{\text{LJ}}} 4\epsilon_{ijab} \left[\left(\frac{\sigma_{ijab}}{r_{ijab}} \right)^{12} - \left(\frac{\sigma_{ijab}}{r_{ijab}} \right)^6 \right] \right. \\
& + \sum_{c=1}^{n_i^{\text{elec}}} \sum_{d=1}^{n_j^{\text{elec}}} \frac{1}{4\pi\epsilon_0} \left[\frac{q_{ic}q_{jd}}{r_{ijcd}} + \frac{q_{ic}\mu_{jd} + q_{jd}\mu_{ic}}{r_{ijcd}^2} \cdot f_1(\omega_i, \omega_j) + \frac{q_{ic}Q_{jd} + q_{jd}Q_{ic}}{r_{ijcd}^3} \cdot f_2(\omega_i, \omega_j) \right. \\
& \left. \left. + \frac{\mu_{ic}\mu_{jd}}{r_{ijcd}^3} \cdot f_3(\omega_i, \omega_j) + \frac{\mu_{ic}Q_{jd} + \mu_{jd}Q_{ic}}{r_{ijcd}^4} \cdot f_4(\omega_i, \omega_j) + \frac{Q_{ic}Q_{jd}}{r_{ijcd}^5} \cdot f_5(\omega_i, \omega_j) \right] \right), \quad (1)
\end{aligned}$$

where ϵ_{ijab} and σ_{ijab} are the LJ energy and size parameters, r_{ijab} and r_{ijcd} are site-site distances, q_{ic} , q_{jd} , μ_{ic} , μ_{jd} , Q_{ic} , and Q_{jd} are the magnitudes of the electrostatic interactions, i.e. the point charges, dipole and quadrupole moments, and the functions $f_k(\omega_i, \omega_j)$ represent dimensionless angle-dependent expressions in terms of the orientations ω_i and ω_j [53].

Thermodynamic properties in heterogeneous systems are very sensitive to a truncation of the intermolecular potential [39, 54–59]. For dispersive interactions, like the LJ potential, various long range correction (LRC) approaches exist which are known to be accurate for planar fluid interfaces [59–67]. The simulations in the present work use slab-based LRC techniques [65–67]. For polar interactions, occasionally even for dispersive interactions [61, 62], LRCs based on Ewald summation are typically employed for the simulation of vapour-liquid interfaces [68–71]. However, a slab-based LRC developed in previous work [57], which evaluates an integral over the density profile, can be used with a high computational efficiency both for non-polar and polar molecular models. In terms of the thermodynamic results, the different methods deliver a similar degree of accuracy for the 2CLJD fluid [30, 70, 71]. Therefore, the slab-based LRC technique is employed here both for dipolar electrostatic interactions and for dispersion. A cutoff radius of 17.5 Å is used (cf. Supplementary Information), and the LRC contribution expressions which are employed in the present work are known to be robust even down to significantly smaller cutoff radii [57].

For the present series of MD simulations, systems were considered where the vapour and liquid phases coexist with each other in direct contact, employing periodic boundary conditions, so that there are two vapour-liquid interfaces which are oriented perpendicular to the y axis. The interfacial tension was computed from the deviation between the normal and the tangential diagonal components of the overall pressure tensor [72, 73], i.e. the mechanical route

$$\gamma = \frac{1}{2} \int_{-\infty}^{\infty} dy (p_N - p_T). \quad (2)$$

Table 1: Molecular models discussed in the present work. The deviations $\delta\rho'$ and δp^s are taken from the referenced publications, and $\delta\gamma$ is the root mean square relative deviation between predictions by the present MD simulations and DIPPR correlations to experimental data [1], determined in the present work. For all considered fluids, the molecular models overestimate γ on average.

Name	Formula	CAS RN	# Model interaction sites	$\delta\rho'$	δp^s	$\delta\gamma$	Source
Acetonitrile	C ₂ H ₃ N	75-05-8	3 LJ + dipole	0.1	4.7	51.7	Deublein <i>et al.</i> [12]
Cyclohexane	C ₆ H ₁₂	110-82-7	6 LJ	0.3	1.7	10.8	Merker <i>et al.</i> [13]
Cyclohexanone	C ₆ H ₁₀ O	108-94-1	7 LJ + dipole	0.9	2.7	26.0	Merker <i>et al.</i> [13]
Cyclohexanol	C ₆ H ₁₀ OH	108-93-0	7 LJ + 3 charges	0.2	3.0	28.3	Merker <i>et al.</i> [15]
Ethylene oxide	C ₂ H ₄ O	75-21-8	3 LJ + dipole	0.4	1.5	16.6	Eckl <i>et al.</i> [7]
Isobutane	C ₄ H ₁₀	75-28-5	4 LJ + dipole + quadrupole	0.6	4.2	12.5	Eckl <i>et al.</i> [8]
Formaldehyde	CH ₂ O	50-00-0	2 LJ + dipole	0.9	4.3	-	Eckl <i>et al.</i> [8]
Dimethyl ether	C ₂ H ₆ O	115-10-6	3 LJ + dipole	0.4	2.6	18.9	Eckl <i>et al.</i> [8]
Sulfur dioxide	SO ₂	7446-09-5	3 LJ + dipole + quadrupole	0.9	4.0	3.4	Eckl <i>et al.</i> [8]
Dimethyl sulfide	C ₂ H ₆ S	75-18-3	3 LJ + dipole + 2 quadrupoles	0.7	4.0	18.1	Eckl <i>et al.</i> [8]
Thiophene	C ₄ H ₁ O	110-02-1	5 LJ + dipole + quadrupole	1.2	3.8	22.4	Eckl <i>et al.</i> [8]
Hydrogen cyanide	HCN	74-90-8	2 LJ + dipole + quadrupole	1.0	7.2	51.9	Eckl <i>et al.</i> [8]
Nitromethane	CH ₃ NO ₂	75-52-5	4 LJ + dipole + quadrupole	0.2	18.7	31.5	Eckl <i>et al.</i> [8]
Phosgene	COCl ₂	75-44-5	4 LJ + dipole + quadrupole	0.5	2.1	17.2	Huang <i>et al.</i> [11]
Benzene	C ₆ H ₆	71-43-2	6 LJ + 6 quadrupoles	0.4	3.4	11.9	Huang <i>et al.</i> [11]
Chlorobenzene	C ₆ H ₅ Cl	108-90-7	7 LJ + dipole + 5 quadrupoles	0.9	5.0	17.8	Huang <i>et al.</i> [11]
Ortho-dichlorobenzene	C ₆ H ₄ Cl ₂	95-50-1	8 LJ + dipole + 4 quadrupoles	0.5	6.4	34.3	Huang <i>et al.</i> [11]
Cyanogen chloride	NCCl	506-77-4	3 LJ + dipole + quadrupole	0.3	2.1	15.3	Miroshnichenko <i>et al.</i> [18]
Cyanogen	C ₂ N ₂	460-19-5	4 LJ + quadrupole	0.6	13.0	2.5	Miroshnichenko <i>et al.</i> [18]
Heptafluoropropane (R227ea)	C ₃ HF ₇	431-89-0	10 LJ + dipole + quadrupole	1.0	1.0	7.2	Eckl <i>et al.</i> [4]
Ammonia	NH ₃	7664-41-7	LJ + 4 charges	0.7	1.6	36.7	Eckl <i>et al.</i> [9]
Formic acid	CH ₂ O ₂	64-18-6	3 LJ + 4 charges	0.8	5.1	9.5	Schnabel <i>et al.</i> [5]
Methanol	CH ₃ OH	67-56-1	2 LJ + 3 charges	0.6	1.1	35.3	Schnabel <i>et al.</i> [6]
Dimethylamine	C ₂ H ₇ N	124-40-3	3 LJ + 3 charges	0.4	6.2	28.7	Schnabel <i>et al.</i> [10]
Ethylene glycol	C ₂ H ₆ O ₂	107-21-1	4 LJ + 6 charges	0.8	4.8	32.6	Huang <i>et al.</i> [14]
Water	H ₂ O	7732-18-5	LJ + 3 charges	1.1	7.2	30.7	Huang <i>et al.</i> [14]
Hydrazine	N ₂ H ₄	302-01-2	2 LJ + 6 charges	0.5	7.6	29.2	Elts <i>et al.</i> [16]
Methylhydrazine	CH ₆ N ₂	60-34-4	3 LJ + 3 charges	0.2	7.0	—	Elts <i>et al.</i> [16]
1,1-Dimethylhydrazine	C ₂ H ₈ N ₂	57-14-7	4 LJ + 3 charges	1.3	3.7	—	Elts <i>et al.</i> [16]
Ethyl acetate	C ₄ H ₈ O ₂	141-78-6	6 LJ + 5 charges	0.1	4.6	10.3	Eckelsbach <i>et al.</i> [19]
Decafluorobutane	C ₄ F ₁₀	355-25-9	14 LJ + 14 charges	0.5	3.5	10.3	Köster <i>et al.</i> [17]
Hexamethyldisiloxane	C ₆ H ₁₈ OSi ₂	107-46-0	9 LJ + 3 charges	0.5	5.0	12.9	Thol <i>et al.</i> [20]
Octamethylcyclotetrasiloxane	C ₈ H ₂₄ O ₂ Si ₄	556-67-2	16 LJ + 8 charges	0.5	6.0	10.5	Thol <i>et al.</i> [21]

Thereby, the normal pressure p_N is given by the y component of the diagonal of the pressure tensor, and the tangential pressure p_T is determined by averaging over the x and z components of the diagonal of the pressure tensor. The simulations were performed with the MD code *ls1 mardyn* [74] in the canonical ensemble with $N = 16000$ molecules. Further details on the MD simulations are given in the Supplementary Information.

Table 2: Molecular simulation results for the vapour-liquid equilibrium of the pure components from the present work. The numbers in parentheses indicate the statistical uncertainties of the last decimal digits.

T K	p^s MPa	ρ' mol l ⁻¹	ρ'' mol l ⁻¹	γ mN m ⁻¹
Acetonitrile				
300	0.005(4)	18.885(1)	0.002(1)	41.9(15)
370	0.137(38)	17.013(20)	0.053(12)	27.1(6)
440	0.839(90)	14.810(21)	0.307(58)	15.7(30)
510	2.72(14)	11.84(9)	1.09(15)	5.9(3)
Cyclohexane				
280	0.008(6)	9.355(3)	0.003(1)	29.2(12)
335	0.049(8)	8.750(4)	0.017(3)	22.3(13)
390	0.270(33)	8.093(3)	0.090(9)	15.5(10)

445	0.855(34)	7.325(13)	0.273(11)	9.5(7)
510	2.387(93)	6.117(26)	0.834(41)	3.5(4)
Cyclohexanone				
250	0.000(0)	9.902(8)	0.000(0)	50.6(38)
315	0.002(2)	9.327(4)	0.001(1)	40.5(12)
380	0.020(6)	8.741(5)	0.006(1)	30.8(21)
445	0.148(22)	8.118(11)	0.042(5)	22.3(13)
510	0.558(37)	7.423(14)	0.146(9)	14.8(6)
Cyclohexanol				
300	0.000(0)	9.700(22)	0.000(0)	40.3(62)
375	0.009(7)	9.028(4)	0.003(1)	32.0(13)
450	0.122(20)	8.277(3)	0.034(8)	22.9(4)
525	0.633(24)	7.422(13)	0.165(12)	14.0(7)
600	2.093(91)	6.325(20)	0.575(31)	5.7(11)
Ethylene oxide				
180	0.000(0)	23.230(4)	0.000(0)	48.1(33)
245	0.006(4)	21.325(6)	0.004(3)	38.6(23)
310	0.331(68)	19.323(27)	0.145(30)	25.0(13)
375	1.304(57)	16.851(13)	0.495(27)	14.3(19)
440	4.77(40)	13.39(13)	2.16(34)	3.7(11)
Isobutane				
120	0.000(0)	12.654(6)	0.000(0)	37.9(13)
185	0.001(1)	11.539(3)	0.001(1)	26.7(8)
250	0.067(17)	10.383(23)	0.032(7)	17.4(5)
315	0.584(10)	8.983(28)	0.263(16)	9.1(7)
380	2.32(12)	7.112(41)	1.13(12)	2.3(4)
Formaldehyde				
180	0.001(1)	31.984(54)	0.001(1)	51.6(14)
235	0.030(9)	29.228(5)	0.017(5)	36.3(15)
290	0.331(54)	26.222(77)	0.155(20)	24.2(14)
345	1.66(13)	22.594(39)	0.782(66)	12.7(9)

T K	p^s MPa	ρ' mol l ⁻¹	ρ'' mol l ⁻¹	γ mN m ⁻¹
Dimethyl ether				
205	0.016(8)	17.016(5)	0.016(4)	30.0(12)
260	0.205(39)	15.415(53)	0.100(35)	19.8(13)
315	0.95(13)	13.563(13)	0.442(38)	10.9(10)
370	3.34(35)	10.94(12)	1.70(31)	3.6(6)
Sulfur dioxide				
220	0.013(8)	24.771(11)	0.007(4)	39.8(29)
265	0.106(39)	22.923(25)	0.049(14)	29.6(27)
310	0.65(17)	20.932(52)	0.278(74)	20.0(14)
355	1.95(46)	18.48(12)	0.83(19)	11.1(9)
400	4.65(26)	14.87(28)	2.30(25)	3.6(10)
Dimethyl sulfide				
190	0.001(1)	19.996(5)	0.000(0)	48.6(16)
260	0.036(14)	18.300(17)	0.022(14)	36.1(10)
330	0.342(26)	16.471(18)	0.134(16)	23.6(7)
400	1.70(15)	14.315(56)	0.635(65)	11.8(13)
470	5.32(33)	10.85(26)	2.60(57)	2.1(8)
Thiophene				
250	0.002(1)	13.107(7)	0.001(1)	43.6(22)
320	0.035(16)	12.168(6)	0.013(4)	33.3(7)
390	0.263(37)	11.166(7)	0.084(9)	22.4(13)
460	1.12(11)	10.001(16)	0.342(35)	13.6(10)
530	3.13(29)	8.458(65)	1.01(16)	5.0(8)
Hydrogen cyanide				
280	0.038(21)	25.756(38)	0.021(11)	34.0(11)
315	0.122(12)	24.015(12)	0.063(10)	25.5(21)
340	0.343(32)	22.589(23)	0.153(23)	19.2(12)
375	0.949(50)	20.50(12)	0.431(41)	13.2(17)
410	2.03(10)	17.766(69)	1.00(12)	7.6(7)
Nitromethane				
260	0.001(1)	19.569(16)	0.001(1)	55.3(37)
330	0.030(7)	18.014(6)	0.014(6)	41.6(34)
400	0.109(22)	16.259(52)	0.044(15)	28.3(14)
470	0.826(69)	14.337(25)	0.266(32)	16.5(15)
540	2.84(26)	11.70(20)	1.06(15)	6.0(9)
Phosgene				
160	0.000(0)	17.047(11)	0.000(0)	49.2(32)
225	0.007(7)	15.578(10)	0.004(3)	34.8(17)
290	0.133(34)	14.047(7)	0.058(8)	23.1(21)
355	0.937(36)	12.311(20)	0.367(8)	12.5(12)
420	3.35(33)	9.873(48)	1.46(22)	3.7(7)

T K	p^s MPa	ρ' mol l ⁻¹	ρ'' mol l ⁻¹	γ mN m ⁻¹
Benzene				
290	0.007(7)	11.208(13)	0.003(3)	33.2(13)
350	0.092(23)	10.403(7)	0.033(3)	24.3(7)
410	0.423(47)	9.523(3)	0.137(16)	15.7(10)
470	1.441(67)	8.450(19)	0.468(22)	8.5(11)
530	3.337(92)	6.884(36)	1.21(13)	2.6(9)
Chlorobenzene				
250	0.004(3)	10.320(8)	0.002(2)	46.7(28)
335	0.011(6)	9.466(11)	0.005(3)	33.3(19)
420	0.122(13)	8.567(23)	0.037(2)	21.9(8)
505	0.79(14)	7.520(30)	0.222(44)	11.7(9)
590	2.91(8)	5.992(20)	0.94(7)	3.2(9)
Ortho-dichlorobenzene				
375	0.003(2)	8.472(5)	0.001(1)	36.1(51)
470	0.097(17)	7.631(3)	0.026(6)	23.4(8)
565	0.701(89)	6.647(16)	0.173(28)	12.6(15)
660	2.79(14)	5.240(33)	0.807(80)	3.0(7)
Cyanogen chloride				
280	0.079(21)	19.777(13)	0.036(8)	28.3(21)
315	0.312(36)	18.490(46)	0.135(9)	21.6(16)
350	0.86(17)	17.08(39)	0.361(83)	14.9(21)
385	1.86(43)	15.27(7)	0.79(23)	9.4(17)
420	3.74(36)	12.92(9)	1.86(54)	4.2(7)
Cyanogen				
260	0.094(31)	18.030(33)	0.049(21)	21.9(24)
290	0.349(95)	16.866(58)	0.168(25)	16.6(12)
320	0.79(30)	15.546(99)	0.36(17)	11.5(16)
350	2.17(34)	13.820(16)	1.04(26)	5.7(6)
380	4.40(5)	11.15(28)	2.89(40)	1.2(6)
Heptafluoropropane				
200	0.002(1)	10.364(13)	0.001(1)	21.9(10)
250	0.063(10)	9.381(8)	0.031(2)	14.8(19)
300	0.466(39)	8.215(3)	0.213(21)	7.7(9)
350	1.776(68)	6.531(20)	0.938(46)	1.8(6)
Ammonia				
220	0.029(2)	41.985(19)	0.015(1)	55.1(19)
260	0.233(38)	38.927(14)	0.116(23)	40.1(36)
300	1.029(80)	35.470(30)	0.467(39)	26.2(13)
340	3.080(66)	31.410(26)	1.421(43)	15.2(25)
380	7.23(15)	25.572(21)	3.86(21)	4.8(1)

T K	p^s MPa	ρ' mol l ⁻¹	ρ'' mol l ⁻¹	γ mN m ⁻¹
Formic acid				
300	0.014(10)	26.192(5)	0.007(2)	39.3(29)
360	0.072(9)	24.478(9)	0.038(14)	30.2(23)
420	0.333(28)	22.607(11)	0.169(20)	22.0(15)
480	1.14(17)	20.36(17)	0.543(61)	15.3(13)
540	3.20(25)	17.45(14)	1.57(18)	6.7(15)
Methanol				
245	0.001(1)	26.175(9)	0.001(1)	36.0(16)
320	0.045(17)	23.958(6)	0.020(7)	27.1(16)
395	0.58(13)	21.317(36)	0.359(49)	14.0(20)
470	3.61(14)	17.318(91)	1.61(26)	6.0(14)
Dimethylamine				
210	0.003(1)	16.653(10)	0.002(1)	35.2(13)
260	0.033(11)	15.523(4)	0.016(6)	27.3(4)
310	0.257(24)	14.279(7)	0.109(10)	19.0(2)
360	1.04(10)	12.888(6)	0.407(45)	11.8(9)
410	2.65(74)	10.814(77)	1.07(50)	5.3(18)
Ethylene glycol				
380	0.005(3)	16.867(29)	0.002(1)	65.6(21)
480	0.107(60)	15.527(25)	0.028(11)	42.3(36)
580	1.144(52)	13.759(14)	0.268(9)	23.6(31)
680	5.45(58)	10.906(97)	1.44(19)	6.2(12)
Water				
300	0.006(5)	56.348(12)	0.002(1)	94.0(21)
375	0.069(16)	52.650(12)	0.024(8)	75.1(13)
450	0.63(10)	48.475(11)	0.31(13)	56.9(19)
525	3.31(16)	43.412(11)	0.94(6)	34.1(21)
600	10.43(20)	36.485(46)	3.28(3)	13.7(20)
Hydrazine				
280	0.000(0)	32.321(8)	0.000(0)	96.7(23)
360	0.028(10)	29.955(5)	0.010(5)	72.6(13)
440	0.358(24)	27.220(18)	0.153(19)	49.4(30)
520	2.24(64)	24.063(80)	1.16(33)	29.9(20)
Methylhydrazine				
270	0.009(5)	19.384(10)	0.004(3)	57.3(13)
345	0.031(13)	17.944(6)	0.012(3)	43.1(16)
420	0.420(64)	16.358(48)	0.137(40)	29.7(12)
495	1.93(21)	14.598(16)	0.573(51)	16.7(8)
570	5.21(22)	12.21(12)	1.73(13)	5.7(9)

T K	p^s MPa	ρ' mol l ⁻¹	ρ'' mol l ⁻¹	γ mN m ⁻¹
1,1-Dimethylhydrazine				
260	0.003(2)	13.783(6)	0.001(1)	35.5(21)
315	0.045(13)	12.833(4)	0.018(6)	27.6(16)
370	0.290(14)	11.806(6)	0.101(9)	19.4(9)
425	1.03(13)	10.603(3)	0.344(40)	11.9(4)
480	2.97(19)	9.026(33)	1.10(12)	4.6(4)
Ethyl acetate				
190	0.000(0)	11.726(4)	0.000(0)	42.2(19)
265	0.002(1)	10.709(18)	0.001(1)	29.9(6)
340	0.063(12)	9.636(10)	0.024(3)	19.7(9)
415	0.497(39)	8.379(6)	0.170(6)	10.9(12)
490	2.078(53)	6.584(19)	0.831(37)	3.0(7)
Decafluorobutane				
260	0.077(13)	6.848(12)	0.038(7)	11.8(17)
310	0.357(6)	6.021(28)	0.157(5)	6.5(6)
360	1.329(67)	4.852(77)	0.657(43)	1.7(3)
Hexamethyldisiloxane				
210	0.000(0)	5.211(31)	0.000(0)	26.3(17)
280	0.002(1)	4.788(5)	0.001(0)	18.4(9)
350	0.047(15)	4.327(8)	0.017(4)	12.1(11)
420	0.299(20)	3.771(10)	0.097(10)	6.7(4)
490	1.161(26)	3.020(25)	0.421(10)	1.8(2)
Octamethylcyclotetrasiloxane				
310	0.000(0)	3.135(14)	0.000(0)	18.6(33)
355	0.004(2)	2.970(12)	0.001(0)	14.6(10)
420	0.044(14)	2.709(8)	0.013(4)	10.1(11)
485	0.217(15)	2.403(12)	0.061(4)	5.7(2)
550	0.699(12)	1.985(27)	0.211(7)	1.9(3)

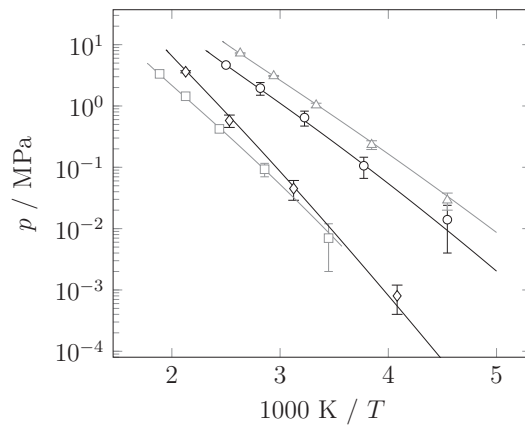


Figure 1: Vapour pressure curves of ammonia, methanol, sulfur dioxide, and benzene. Solid lines represent correlations to experimental data [76–79], and symbols are the present simulation results: Sulfur dioxide (\circ), benzene (\square), ammonia (\triangle), and methanol (\diamond).

3. Results and Discussion

Tab. 1 gives an overview of the molecular models investigated in the present work. All studied models are rigid, i.e. internal degrees of freedom are not accounted for. The deviations $\delta\rho'$ and δp^S , which are reported for the models in Tab. 1, are taken from the corresponding publications and represent relative mean deviations of the simulated values from correlations to experimental data [4–21]. The molecular simulations in previous work were performed with the Grand Equilibrium method [75].

Fig. 1 shows the simulation results for the vapour pressure of ammonia, methanol, sulfur dioxide, and benzene from the present work which were obtained from heterogeneous simulations; cf. Tab. 2 for the numerical simulation results. The present results for the saturated densities and the vapour pressure are in very good agreement with experimental data [76–79]. However, for low temperatures, the uncertainties in the saturated vapour density and vapour pressure are relatively high. This is due to the fact that at low temperatures, in many cases, less than one molecule is in the vapour phase on average, which yields relatively high statistical uncertainties. Similar findings were obtained for the other fluids studied in the present work. The simulation results obtained for the vapour pressure and the saturated densities for all studied fluids are reported in Tab. 2 together with the data for the surface tension.

The relative mean deviation $\delta\gamma$ between the simulation data and the experimental data reported in Tab. 1 is calculated in the same way as the deviations for the saturated liquid density and the vapour pressure. It represents the root mean square deviation of the surface tension predicted by the molecular models from Design Institute for Physical Properties (DIPPR) correlations to experimental data

$$|\delta\gamma| = \sqrt{\frac{1}{K} \sum_{i=1}^K \left(\frac{\gamma^{\text{sim}}(T_i) - \gamma^{\text{exp}}(T_i)}{\gamma^{\text{exp}}(T_i)} \right)^2}, \quad (3)$$

over a set of K simulation results at temperatures between the triple point temperature and 95 % of the critical temperature. By convention, the sign of $\delta\gamma$ is positive if, on average, the model overestimates the surface tension ($\delta\gamma = +|\delta\gamma|$) and negative otherwise ($\delta\gamma = -|\delta\gamma|$). Underlying experimental surface tension data are usually not available over the entire temperature range. Only for four compounds – water, methanol, ammonia, and heptafluoropropane – experimental data are available over the entire temperature range. In most cases, the surface tension is measured only up to 373 K and the DIPPR correlation extrapolates these results to the critical point [1, 2].

The DIPPR correlations usually agree with available experimental data within 3 %, only for dimethyl sulfide, ortho-dichlorobenzene, heptafluoropropane, cyanogen, decafluorobutane, and hexamethyldisiloxane deviations of up to 5 % are reported [1]. For three fluids – formaldehyde, methylhydrazine, and 1,1-dimethylhydrazine – no experimental data are available. The DIPPR correlations do not match the critical temperature for ethylene glycol and formic acid. Therefore, a straight line is used to connect the DIPPR correlation and the critical point of respective fluids.

Figs. 2 and 3 show the surface tension for some of the studied fluids as a function of the temperature (for the other fluids: cf. Supplementary Information). The molecular simulation results are compared with DIPPR correlations to experimental data. For formaldehyde, methylhydrazine and 1,1-dimethylhydrazine experimental data are available. The predictions of the surface tension agree reasonably well with the experimental data. Fig. 4 shows the surface tension predicted by MD simulation as a function of the experimental surface tension calculated by the DIPPR correlation [1] for all studied fluids. The molecular models overestimate the surface tension in all cases. The average deviation between the predictions by the molecular simulation and the experimental data is about 20 %. This is in line with results for the surface tension obtained by molecular simulation in the literature [30–40]. Compared to other methods for predicting the surface tension of low-molecular fluids, molecular modelling and simulation, using models which are adjusted to bulk data, leads to relatively high deviations.

Several examples illustrate this: The surface tension of benzene is reproduced with a deviation of $|\delta\gamma| \approx 4\%$ using the corresponding-states (CS) correlation by Sastry and Rao [45], $|\delta\gamma| = 1\%$ with the CS correlation by Zuo and Stenby [44], and $|\delta\gamma| = 8.5\%$ from a parachor correlation [42–44]; the molecular model from Huang *et al.* [11] has $|\delta\gamma| = 11.9\%$. For cyclohexane, $|\delta\gamma| \approx 1\%$ is obtained following CS

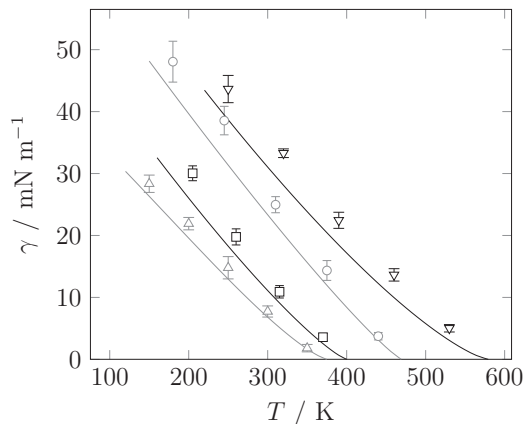


Figure 2: Surface tension as a function of the temperature. Solid lines represent DIPPR correlations to experimental data [1], and symbols are the present simulation results: Thiophene (∇), ethylene oxide (\circ), dimethyl ether (\square), and heptafluoropropane (\triangle).

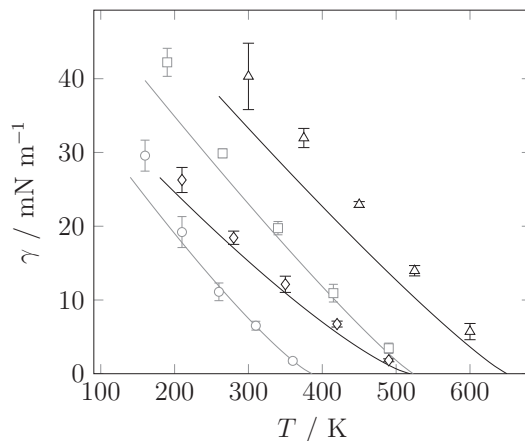


Figure 3: Surface tension as a function of the temperature. Solid lines represent DIPPR correlations to experimental data [1], and symbols are the present simulation results: Cyclohexanol (\triangle), ethyl acetate (\square), hexamethyldisiloxane (\diamond), and decafluorobutane (\circ).

by Sastry and Rao [45], $|\delta\gamma| = 0.7\%$ with CS by Zuo and Stenby [44], $|\delta\gamma| = 7.4\%$ from the parachor correlation [42–44], and $|\delta\gamma| = 10.8\%$ with the molecular model from Merker *et al.* [13]. In case of ethyl acetate, a CS correlation yields $|\delta\gamma| \approx 7\%$ [45] and density functional theory with the PC-SAFT equation of state [48] reaches $|\delta\gamma| \approx 4\%$, whereas the average relative deviation is $|\delta\gamma| = 10.3\%$ for the molecular model from Eckelsbach *et al.* [19]. For methanol, the CS correlation by Sastry and Rao [45] exhibits almost perfect agreement $|\delta\gamma| < 1\%$; the molecular model by Schnabel *et al.* [6] has $|\delta\gamma| = 35.3\%$. Zuo and Stenby [44] reproduce the surface tension of isobutane with an accuracy of $|\delta\gamma| = 1.6\%$ using their CS correlation and with $|\delta\gamma| = 2.5\%$ using a parachor correlation [42–44]; in contrast, the molecular model for isobutane from Eckl *et al.* [8] exhibits a deviation of $|\delta\gamma| = 12.5\%$.

Square gradient theory with the SAFT-VR Mie equation of state, following Garrido *et al.* [46], typically yields deviations of the order of 2 to 3% for the surface tension of low-molecular fluids. However, no direct comparison is possible with any of the present results.

The anisotropic united atom (AUA) force field [80, 81] was also adjusted to bulk data only. All results for γ from simulations with AUA models are therefore predictions of interfacial properties from bulk fluid properties. For benzene, applying the test-area method in Monte Carlo simulations with the AUA-9 sites

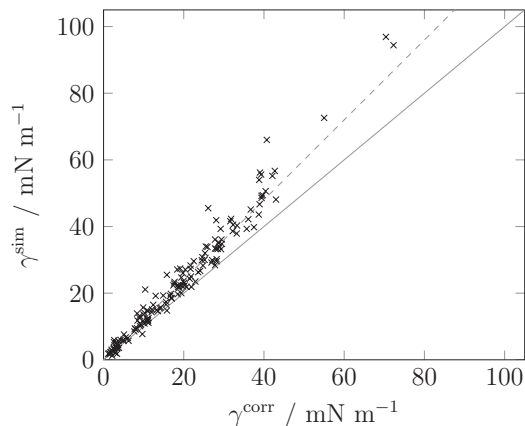


Figure 4: Predicted surface tension γ^{sim} over the experimental surface tension γ^{corr} based on DIPPR correlations [1] for the present molecular simulation results. The solid line represents perfect agreement between simulation and experiment, and the dashed line represents a deviation of 20 %.

force field, which was parameterized by Nieto Draghi and collaborators [82, 83], Biscay *et al.* [84] report a surface tension which deviates from experimental data by about $\delta\gamma \approx +4\%$, compared to $\delta\gamma = +11.9\%$ for the Huang *et al.* [11] model. For cyclohexane [84], the AUA-9 sites model has $\delta\gamma \approx +5\%$, whereas for the Merker *et al.* [13] model, $\delta\gamma = +11.9\%$ was found in the present work. The AUA-4 model [81] underestimates the surface tension of methanol by $\delta\gamma \approx -12\%$, cf. Biscay *et al.* [85], which compares favourably to the Schnabel *et al.* [6] model with $\delta\gamma = +35.3\%$. Overall, the AUA force field is more reliable for predicting the surface tension than the models investigated in the present work [86]; it has roughly the same accuracy as empirical parachor correlations [44]. However, this still makes the AUA force field less accurate than empirical CS correlations [44, 45] and semiempirical square gradient theory [46].

Since molecular simulation is also computationally much more expensive than the other approaches, it cannot be recommended to predict interfacial properties from molecular models which were not previously adjusted to or, at least, validated against such data. However, a systematic overestimation of the surface tension has also been observed in density functional theory in combination with physically based equations of state [47, 87–90]. To account for this overestimation, an empirical correction expression is often employed, which is formally attributed to the presence of capillary waves and decreases the surface tension. Without this correction term, which was adjusted to fit the experimental surface tension values of the n-alkane series [47], density functional theory would deviate from the surface tension of real fluids in a similar way as the molecular models mentioned above. In square gradient theory, the influence parameter, which controls the magnitude of the surface excess free energy, is also adjusted to surface tension data.

The unfavourable performance of molecular models, compared to methods which are more abstract physically and less expensive numerically, is explained by the fact that the molecular models are *entirely* predictive for interfacial properties. All other methods, i.e. density functional theory, square gradient theory, and phenomenological correlations, were adjusted to surface tension data at least indirectly. Moreover, methods which are based on analytical equations of state, including molecular equations of state, fail in the vicinity of the critical point, so that $\delta\gamma$ diverges at high temperatures. Renormalization group theory has to be employed in these cases to avoid unphysical behaviour [48, 91, 92]. By molecular simulation, the (Ising class) critical scaling behaviour of intermolecular pair potentials is correctly captured. Therefore, any fit of force-field parameters to VLE data over a significant temperature range always indirectly adjusts the molecular model to the critical temperature [93].

It has been shown before that a better agreement of molecular simulation results with experimental data for the surface tension can be achieved by taking into account experimental data on the surface tension in the parameterization of the molecular models. However, improvements in the quality of the representation of the surface tension have to be traded off against losses in the quality of the representation of bulk fluid

properties [31, 93–95].

4. Conclusion

In the present work, the surface tension of 33 real molecular fluids was determined by MD simulation. These models were parameterized to reproduce the saturated liquid density, the vapour pressure, and the enthalpy of vaporization. Accordingly, bulk properties of the fluid models from molecular simulations agree well with experimental data for the real fluids. On the basis of well-described phase equilibria, the model predictions for the surface tension were assessed. It was found that the surface tension is consistently overpredicted by the molecular models. On average, the deviation is about +20 %.

Acknowledgment

The authors acknowledge financial support from BMBF within the *SkaSim* project (grant no. 01H13005A) and from Deutsche Forschungsgemeinschaft (DFG) within the Collaborative Research Centre (SFB) 926, subproject A01. They thank Patrick Leidecker for performing some of the present simulations and Gabriela Guevara Carrión, Marco Hülsmann, Maximilian Kohns, Erich A. Müller, Yonny Mauricio Muñoz Muñoz, Jayant Kumar Singh and Jadran Vrabec for fruitful discussions. The present work was conducted under the auspices of the Boltzmann-Zuse Society for Computational Molecular Engineering (BZS), and the simulations were carried out on *elwetritsch* at the Regional University Computing Centre Kaiserslautern (RHRK) under the grant *TUKL-MSWS* and on *SuperMUC* at Leibniz Supercomputing Centre (LRZ), Garching, within the *Sparlampe* computing project (pr48te).

- [1] R. L. Rowley, W. V. Wilding, J. L. Oscarson, Y. Yang, N. A. Zundel, T. E. Daubert, R. P. Danner, *DIPPR Information and Data Evaluation Manager for the Design Institute for Physical Properties*, AIChE, 2013, Version 7.0.0.
- [2] *DDB - Dortmund Data Bank*, 7.3.0.458 (DDB), 1.18.0.122 (Artist), DDBST GmbH, Oldenburg, 2015.
- [3] A. Ghoufi, P. Malfreyt, D. J. Tildesley, Computer modelling of the surface tension of the gas-liquid and liquid-liquid interface, *Chem. Soc. Rev.* 45 (2016) 1387–1409.
- [4] B. Eckl, Y.-L. Huang, J. Vrabec, H. Hasse, Vapor pressure of R227ea + ethanol at 343.13 K by molecular simulation, *Fluid Phase Equilib.* 260 (2007) 177–182.
- [5] T. Schnabel, M. Cortada, J. Vrabec, S. Lago, H. Hasse, Molecular model for formic acid adjusted to vapor-liquid equilibria, *Chem. Phys. Lett.* 435 (2007) 268–272.
- [6] T. Schnabel, A. Srivastava, J. Vrabec, H. Hasse, Hydrogen bonding of methanol in supercritical CO₂: Comparison between ¹H NMR spectroscopic data and molecular simulation results, *J. Phys. Chem. B*, 111 (2007) 9871–9878.
- [7] B. Eckl, J. Vrabec, H. Hasse, On the application of force fields for predicting a wide variety of properties: Ethylene oxide as an example, *Fluid Phase Equilib.* 274 (2008) 16–26.
- [8] B. Eckl, J. Vrabec, H. Hasse, Set of molecular models based on quantum mechanical ab initio calculations and thermodynamic data, *J. Phys. Chem. B* 112 (2008) 12710–12721.
- [9] B. Eckl, J. Vrabec, H. Hasse, An optimised molecular model for ammonia, *Mol. Phys.* 106 (2008) 1039–1046.
- [10] T. Schnabel, J. Vrabec, H. Hasse, Molecular simulation study of hydrogen bonding mixtures and new molecular models for mono- and dimethylamine, *Fluid Phase Equilib.* 263 (2008) 144–159.
- [11] Y.-L. Huang, M. Heilig, H. Hasse, J. Vrabec, Vapor-liquid equilibria of hydrogen chloride, phosgene, benzene, chlorobenzene, ortho-dichlorobenzene, and toluene by molecular simulation, *AIChE J.* 52 (2011) 1043–1060.
- [12] S. Deublein, P. Metzler, J. Vrabec, H. Hasse, Automated development of force fields for the calculation of thermodynamic properties: Acetonitrile as a case study, *Mol. Sim.* 39 (2012) 109–118.
- [13] T. Merker, J. Vrabec, H. Hasse, Molecular simulation study on the solubility of carbon dioxide in mixtures of cyclohexane + cyclohexanone, *Fluid Phase Equilib.* 315 (2012) 77–83.
- [14] Y.-L. Huang, T. Merker, M. Heilig, H. Hasse, J. Vrabec, Molecular modeling and simulation of vapor-liquid equilibria of ethylene oxide, ethylene glycol, and water as well as their binary mixtures, *Ind. Eng. Chem. Res.* 51 (2012) 7428–7440.
- [15] T. Merker, J. Vrabec, H. Hasse, Engineering molecular models: Efficient parametrization procedure and cyclohexanol as case study, *Soft Mater.* 10 (2012) 3–24.
- [16] E. Elts, T. Windmann, D. Staak, J. Vrabec, Fluid phase behavior from molecular simulation: Hydrazine, monomethylhydrazine, dimethylhydrazine and binary mixtures containing these compounds, *Fluid Phase Equilib.* 322–323 (2012) 79–91.
- [17] A. Köster, P. Nandi, T. Windmann, D. Ramjugernath, J. Vrabec, Vapor-liquid equilibria of ethylene (C₂H₄) + decafluorobutane (C₄F₁₀) at 268 to 298 K from experiment, molecular simulation and the Peng-Robinson equation of state, *Fluid Phase Equilib.* 336 (2012) 104–112.
- [18] S. Miroshnichenko, T. Grützner, D. Staak, J. Vrabec, Molecular simulation of the vapor-liquid phase behavior of cyanides and their binary mixtures, *Fluid Phase Equilib.* 354 (2013) 286–297.

- [19] S. Eckelsbach, T. Janzen, A. Köster, S. Miroshnichenko, Y. M. Muñoz Muñoz, J. Vrabec, Molecular models for cyclic alkanes and ethyl acetate as well as surface tension data from molecular simulation, in W. E. Nagel, D. B. Kröner, M. M. Resch (eds.), *High Performance Computing in Science and Engineering '14*, pp. 645–649. Springer, Heidelberg, 2014.
- [20] M. Thol, F. H. Dubberke, G. Rutkai, T. Windmann, A. Köster, R. Span, J. Vrabec, Fundamental equation of state correlation for hexamethyldisiloxane based on experimental and molecular simulation data, *Fluid Phase Equilib.* 416 (2016) 133–151.
- [21] M. Thol, G. Rutkai, A. Köster, F. H. Dubberke, T. Windmann, R. Span, J. Vrabec, Thermodynamic properties of octamethylcyclotetrasiloxane, *J. Chem. Eng. Data* 61 (2016) 2580–2595.
- [22] G. Guevara Carrión, J. Vrabec, H. Hasse, Prediction of transport properties of liquid ammonia and its binary mixture with methanol by molecular simulation, *Int. J. Thermophys.* 33 (2012) 449–468.
- [23] S. Pañez, G. Guevara Carrión, H. Hasse, J. Vrabec, Mutual diffusion in the ternary mixture water + methanol + ethanol and its binary subsystems, *Phys. Chem. Chem. Phys.* 15 (2013) 3985–4001.
- [24] G. Guevara Carrión, J. Vrabec, H. Hasse, Prediction of self-diffusion coefficient and shear viscosity of water and its binary mixtures with methanol and ethanol by molecular simulation, *J. Chem. Phys.* 134 (2011) 074508.
- [25] G. Guevara Carrión, J. Vrabec, H. Hasse, On the prediction of transport properties of monomethylamine, dimethylamine, dimethylether and hydrogen chloride by molecular simulation, *Fluid Phase Equilib.* 316 (2012) 46–54.
- [26] G. Guevara Carrión, T. Janzen, Y. M. Muñoz Muñoz, J. Vrabec, Mutual diffusion of binary liquid mixtures containing methanol, ethanol, acetone, benzene, cyclohexane, toluene and carbon tetrachloride, *J. Chem. Phys.* 144 (2016) 124501.
- [27] M. Thol, G. Rutkai, A. Köster, M. Kortmann, R. Span, J. Vrabec, Fundamental equation of state for ethylene oxide based on a hybrid dataset, *Chem. Eng. Sci.* 121 (2015) 87–99.
- [28] G. Rutkai, J. Vrabec, Empirical fundamental equation of state for phosgene based on molecular simulation data, *J. Chem. Eng. Data* 60 (2015) 2895–2905.
- [29] S. Werth, M. Horsch, H. Hasse, Surface tension of the two center Lennard-Jones plus quadrupole model fluid, *Fluid Phase Equilib.* 392 (2015) 12–18.
- [30] S. Werth, M. Horsch, H. Hasse, Surface tension of the two center Lennard-Jones plus point dipole fluid, *J. Chem. Phys.* 144 (2016) 054702.
- [31] S. Werth, K. Stöbener, P. Klein, K.-H. Küfer, M. Horsch, H. Hasse, Molecular modelling and simulation of the surface tension of real quadrupolar fluids, *Chem. Eng. Sci.* 121 (2015) 110–117.
- [32] J.-C. Neyt, A. Wender, V. Lachet, P. Malfreyt, Prediction of the temperature dependence of the surface tension of SO₂, N₂, O₂, and Ar by Monte Carlo molecular simulations, *J. Phys. Chem. B*, 115 (2011) 9421–9430.
- [33] S. Eckelsbach, S. Miroshnichenko, G. Rutkai, J. Vrabec, Surface tension, large scale thermodynamic data generation and vapor-liquid equilibria of real compounds, in W. E. Nagel, D. B. Kröner, M. M. Resch (eds.), *High Performance Computing in Science and Engineering '13*, pp. 635–646, Springer, Heidelberg, 2013.
- [34] C. Avendaño, T. Lafitte, A. Galindo, C. S. Adjiman, G. Jackson, E. A. Müller, SAFT- γ force field for the simulation of molecular fluids. 1. A single-site coarse grained model of carbon dioxide, *J. Phys. Chem. B* 115 (2011) 11154–11169.
- [35] C. Herdes, T. S. Totton, E. A. Müller, Coarse grained force field for the molecular simulation of natural gases and condensates, *Fluid Phase Equilib.* 406 (2015) 91–100, 2015.
- [36] N. Ferrando, V. Lachet, J. Pérez Pellitero, A. D. Mackie, P. Malfreyt, A transferable force field to predict phase equilibria and surface tension of ethers and glycol ethers, *J. Phys. Chem. B* 115 (2011) 10654–10664.
- [37] S. Eckelsbach, J. Vrabec, Fluid phase interface properties of acetone, oxygen, nitrogen and their binary mixtures by molecular simulation, *Phys. Chem. Chem. Phys.* 17 (2015) 27195–27203.
- [38] S. K. Singh, A. Sinha, G. Deo, J. K. Singh, Vapor-liquid phase coexistence, critical properties, and surface tension of confined alkanes, *J. Phys. Chem. C* 113 (2009) 7170–7180.
- [39] R. A. Zubillaga, A. Labastida, B. Cruz, J. C. Martínez, E. Sánchez, J. Alejandre, Surface tension of organic liquids using the OPLS/AA force field, *J. Chem. Theory Comput.* 9 (2013) 1611–1615.
- [40] C. Caleman, P. J. van Maaren, M. Hong, J. S. Hub, L. T. Costa, D. van der Spoel, Force field benchmark of organic liquids: Density, enthalpy of vaporization, heat capacities, surface tension, isothermal compressibility, volumetric expansion coefficient, and dielectric constant, *J. Chem. Theory Comput.* 8 (2012) 61–74.
- [41] S. Sugden, A relation between surface tension, density, and chemical composition, *J. Chem. Soc.* 125 (1924) 1177–1189.
- [42] J. A. Hugill, A. J. van Walsenes, Surface tension: A simple correlation for natural gas + condensate systems, *Fluid Phase Equilib.* 29 (1986) 383–390.
- [43] K. A. M. Gasem, P. B. Dulcamara Jr., K. B. Dickson, R. L. Robinson Jr., Test of prediction methods for interfacial tensions of CO₂ and ethane in hydrocarbon solvents, *Fluid Phase Equilib.* 53 (1989) 39–50.
- [44] Y.-X. Zuo, E. H. Stenby, Corresponding-states and parachor models for the calculation of interfacial tensions, *Canad. J. Chem. Eng.* 75 (1997) 1130–1137.
- [45] S. R. S. Sastry, K. K. Rao, A simple method to predict surface tension of organic liquids, *Chem. Eng. J.* 59 (1995) 181–186.
- [46] J. M. Garrido, M. M. Piñeiro, F. J. Blas, E. A. Müller, Interfacial tensions of industrial fluids from a molecular-based square gradient theory, *AIChE J.* 62 (2016) 1781–1794.
- [47] J. Groß, A density functional theory for vapor-liquid interfaces using the PCP-SAFT equation of state, *J. Chem. Phys.* 131 (2009) 204705.
- [48] X. Tang, J. Groß, Density functional theory for calculating surface tensions with a simple renormalization formalism for the critical point, *J. Supercrit. Fluids* 55 (2010) 735–742.
- [49] J. Groß, G. Sadowski, Perturbed-Chain SAFT: An equation of state based on a perturbation theory for chain molecules, *Ind. Eng. Chem. Res.* 44 (2001) 1244–1260.

- [50] J. Groß, J. Vrabec, An equation-of-state contribution for polar components: Dipolar molecules, *AIChE J.* 52 (2006) 1194–1204.
- [51] J. Vrabec, J. Groß, Vapor-liquid equilibria simulation and an equation of state contribution for dipole-quadrupole interactions, *J. Phys. Chem. B* 112 (2008) 51–60.
- [52] C. Avendaño, T. Lafitte, C. S. Adjiman, A. Galindo, E. A. Müller, G. Jackson, SAFT- γ force field for the simulation of molecular fluids: 2. Coarse-grained models of greenhouse gases, refrigerants, and long alkanes, *J. Phys. Chem. B* 117 (2013) 2717–2733.
- [53] C. G. Gray, K. E. Gubbins, *Theory of Molecular Fluids*, vol. 1 (Fundamentals), Clarendon, Oxford, 1984.
- [54] F. Goujon, P. Malfreyt, D. J. Tildesley, The gas-liquid surface tension of argon: A reconciliation between experiment and simulation, *J. Chem. Phys.* 140 (2014) 244710.
- [55] S. Werth, M. Horsch, J. Vrabec, H. Hasse, Comment on ‘The gas-liquid surface tension of argon: A reconciliation between experiment and simulation,’ *J. Chem. Phys.* 142 (2015) 107101.
- [56] F. Goujon, P. Malfreyt, D. J. Tildesley, Response to Comment on ‘The gas-liquid surface tension of argon: A reconciliation between experiment and simulation,’ *J. Chem. Phys.* 142 (2015) 107102.
- [57] S. Werth, M. Horsch, H. Hasse, Long-range correction for dipolar fluids at planar interfaces, *Mol. Phys.* 113 (2015) 3750–3756.
- [58] F. Goujon, P. Malfreyt, J.-M. Simon, A. Boutin, B. Rousseau, A. H. Fuchs, Monte Carlo versus molecular dynamics simulations in heterogeneous systems: an application to the n-pentane liquid-vapor interface, *J. Chem. Phys.* 121 (2004) 12559–12571.
- [59] A. Trokhymchuk, J. Alejandre, Computer simulations of liquid/vapor interface in Lennard-Jones fluids: Some questions and answers, *J. Chem. Phys.* 111 (1999) 8510–8523.
- [60] P. J. in ‘t Veld, A. E. Ismail, G. S. Grest, Application of Ewald summations to long-range dispersion forces, *J. Chem. Phys.* 127 (2007) 144711.
- [61] R. E. Isele-Holder, W. Mitchell, A. E. Ismail, Development and application of a particle-particle particle-mesh Ewald method for dispersion interactions, *J. Chem. Phys.* 137 (2012) 174107.
- [62] R. Isele-Holder, W. Mitchell, J. R. Hammond, A. Kohlmeyer, A. E. Ismail, Reconsidering dispersion potentials: Reduced cutoffs in mesh-based Ewald solvers can be faster than truncation, *J. Chem. Theory Comput.* 9 (2013) 5412–5420.
- [63] G. Mathias, B. Egwolf, M. Nonella, P. Tavan, A fast multipole method combined with a reaction field for long-range electrostatics in molecular dynamics simulations: The effects of truncation on the properties of water, *J. Chem. Phys.* 118 (2003) 10847–10860.
- [64] D. Taveling, P. Springer, P. Bientinesi, A. E. Ismail, Multilevel summation for dispersion: A linear-time algorithm for r^{-6} potentials, *J. Chem. Phys.* 140 (2014) 024105.
- [65] M. Mecke, J. Winkelmann, J. Fischer, Molecular dynamics simulation of the liquidvapor interface: The Lennard-Jones fluid, *J. Chem. Phys.* 107 (1997) 9264–9270.
- [66] J. Janeček, Long range corrections in inhomogeneous simulations, *J. Phys. Chem. B* 110 (2006) 6264–6269.
- [67] S. Werth, G. Rutkai, J. Vrabec, M. Horsch, H. Hasse, Long-range correction for multi-site Lennard-Jones models and planar interfaces, *Mol. Phys.* 112 (2014) 2227–2234.
- [68] J. W. Perram, H. G. Peterson, S. W. de Leeuw, An algorithm for the simulation of condensed matter which grows as the $3/2$ power of the number of particles, *Mol. Phys.* 65 (1988) 875–893.
- [69] R. W. Hockney, J. W. Eastwood, *Computer Simulations Using Particles*, Taylor & Francis, Bristol, PA, USA, 1988.
- [70] S. G. Moore, M. J. Stevens, G. S. Grest, Liquid-vapor interface of the Stockmayer fluid in a uniform external field *Phys. Rev. E* 91 (2015) 022309.
- [71] S. Enders, H. Kahl, M. Mecke, J. Winkelmann, Molecular dynamics simulation of the liquidvapor interface: I. The orientational profile of 2-center Lennard-Jones and of Stockmayer fluid molecules, *J. Mol. Liq.* 115 (2004) 29–39.
- [72] J. P. R. B. Walton, D. J. Tildesley, J. S. Rowlinson, J. R. Henderson, The pressure tensor at the planar surface of a liquid, *Mol. Phys.* 48 (1983) 1357–1368.
- [73] J. G. Kirkwood, F. P. Buff, The statistical mechanical theory of surface tension, *J. Chem. Phys.* 17 (1949) 338–343.
- [74] C. Niethammer, S. Becker, M. Bernreuther, M. Buchholz, W. Eckhardt, A. Heinecke, S. Werth, H.-J. Bungartz, C. W. Glass, H. Hasse, J. Vrabec, M. Horsch, *ls1 mardyn*: The massively parallel molecular dynamics code for large systems, *J. Chem. Theory Comput.* 10 (2014) 4455–4464.
- [75] J. Vrabec, H. Hasse, Grand Equilibrium: Vapour-liquid equilibria by a new molecular simulation method, *Mol. Phys.* 100 (2002) 3375–3383.
- [76] R. Tillner-Roth, F. Harms-Watzenberg, H. D. Baehr, Eine neue Fundamentalgleichung für Ammoniak, *DKV-Tagungsbericht* 20 (1993) 167–181.
- [77] A. Polt, B. Platzler, G. Maurer, The Bender equation of state for 14 polyatomic pure substances, *Chem. Tech. (Leipzig)* 44 (1992) 216–224.
- [78] K. M. de Reuck, R. J. B. Craven, *Methanol, International Thermodynamic Tables of the Fluid State – 12*, Blackwell Scientific, London, 1993.
- [79] E. W. Lemmon, R. Span, Short fundamental equations of state for 20 industrial fluids, *J. Chem. Eng. Data* 51 (2006) 785–850.
- [80] S. Toxvaerd, Molecular dynamics calculation of the equation of state of alkanes, *J. Chem. Phys.* 93 (1990) 4290–4295.
- [81] P. Ungerer, C. Beauvais, J. Delhommelle, A. Boutin, B. Rousseau, A. H. Fuchs, Optimization of the anisotropic united atoms intermolecular potential for n-alkanes, *J. Chem. Phys.* 112 (2000) 5499–5510.
- [82] P. Bonnaud, C. Nieto Draghi, P. Ungerer, Anisotropic united atom model including the electrostatic interactions of benzene, *J. Phys. Chem. B* 111 (2007) 3730–3741.

- [83] C. Nieto Draghi, P. Bonnaud, P. Ungerer, Anisotropic united atom model including the electrostatic interactions of methylbenzenes. I. Thermodynamic and structural properties, *J. Phys. Chem. C* 111 (2007) 15686–15699.
- [84] F. Biscay, A. Ghoufi, V. Lachet, P. Malfreyt, Calculation of the surface tension of cyclic and aromatic hydrocarbons from Monte Carlo simulations using an anisotropic united atom model (AUA), *Phys. Chem. Chem. Phys.* 11 (2009) 6132–6147.
- [85] F. Biscay, A. Ghoufi, V. Lachet, P. Malfreyt, Prediction of the surface tension of the liquid-vapor interface of alcohols from Monte Carlo simulations, *J. Phys. Chem. C* 115 (2011) 8670–8683.
- [86] F. Biscay, A. Ghoufi, F. Goujon, V. Lachet, P. Malfreyt, Surface tensions of linear and branched alkanes from Monte Carlo simulations using the anisotropic united atom model, *J. Phys. Chem. B* 112 (2008) 13885–13897.
- [87] F. Llovel, A. Galindo, F. J. Blas, G. Jackson, Classical density functional theory for the prediction of the surface tension and interfacial properties of fluids mixtures of chain molecules based on the statistical associating fluid theory for potentials of variable range, *J. Chem. Phys.* 133 (2010) 024704.
- [88] P. I. Teixeira, M. M. Telo da Gama, Density-functional theory for the interfacial properties of a dipolar fluid, *J. Phys.: Cond. Mat.* 3 (1991) 111–125.
- [89] J. Winkelmann, The liquid-vapour interface of pure fluids and mixtures: application of computer simulation and density functional theory, *J. Phys.: Cond. Mat.* 13 (2001) 4739–4768.
- [90] P. Frodl, S. Dietrich, Thermal and structural properties of the liquid-vapor interface in dipolar fluids, *Phys. Rev. E* 48 (1993) 3741–3759.
- [91] E. Forte, F. Llovel, L. F. Vega, J. P. M. Trusler, A. Galindo, Application of a renormalization-group treatment to the statistical associating fluid theory for potentials of variable range (SAFT-VR), *J. Chem. Phys.* 134 (2011) 154102.
- [92] E. Forte, F. Llovel, J. P. M. Trusler, A. Galindo, Application of the statistical associating fluid theory for potentials of variable range (SAFT-VR) coupled with renormalization-group (RG) theory to model the phase equilibria and second-derivative properties of pure fluids, *Fluid Phase Equilib.* 337 (2013) 274–287.
- [93] K. Stöbener, P. Klein, M. Horsch, K. Küfer, H. Hasse, Parametrization of two-center Lennard-Jones plus point-quadrupole force field models by multicriteria optimization, *Fluid Phase Equilib.* 411 (2016) 33–42.
- [94] K. Stöbener, P. Klein, S. Reiser, M. Horsch, K.-H. Küfer, H. Hasse, Multicriteria optimization of molecular force fields by Pareto approach, *Fluid Phase Equilib.* 373 (2014) 100–108.
- [95] S. Werth, K. Stöbener, M. Horsch, H. Hasse, Simultaneous description of bulk and interfacial properties of fluids by the Mie potential, *Mol. Phys.*, in press (2016), doi:10.1080/00268976.2016.1206218.

Supplementary information: Molecular simulation of the surface tension of 33 multi-site models for real fluids

Stephan Werth^a, Martin Horsch^{a,*}, Hans Hasse^a

^aUniversity of Kaiserslautern, Laboratory of Engineering Thermodynamics, Erwin-Schrödinger Str. 44, 67663 Kaiserslautern, Germany

Molecular simulation details

The equation of motion was solved by a leapfrog integrator [1] with a time step of $\Delta t = 1$ fs. The elongation of the simulation volume normal to the interface was 30 nm and the thickness of the liquid film in the middle of the simulation volume was 15 nm to account for finite size effects [2]. The elongation in the other spatial directions was at least 10 nm. The equilibration was executed for 500 000 time steps. The production was conducted for 2 500 000 time steps to reduce statistical uncertainties. The statistical errors were estimated to be three times the standard deviation of five block averages, each over 500 000 time steps. The saturated densities and vapour pressures were calculated as an average over the respective phases excluding the area close to the interface, i.e. the area where the first derivative of the density with respect to the y coordinate deviated from zero significantly.

The cutoff radius was set to 17.5 Å and a centre-of-mass cutoff scheme was employed. The LJ interactions were corrected with a slab-based long range correction based on the density profile [3]. Electrostatic long-range interactions were approximated by a resulting effective molecular dipole and corrected with a slab-based long range correction based on the density profile [4]. The quadrupolar interactions do not need a long-range correction as they decay by r^{-10} , cf. Prausnitz *et al.* [5].

- [1] D. Fincham, Leapfrog rotational algorithms, *Mol. Sim.* 8 (1992) 165–178.
- [2] S. Werth, S. V. Lishchuk, M. Horsch, H. Hasse, The influence of the liquid slab thickness on the planar vapor-liquid interfacial tension, *Phys. A* 392 (2013) 2359–2367.
- [3] S. Werth, G. Rutkai, J. Vrabec, M. Horsch, H. Hasse, Long-range correction for multi-site Lennard-Jones models and planar interfaces, *Mol. Phys.* 112 (2014) 2227–2234.
- [4] S. Werth, M. Horsch, H. Hasse, Long-range correction for dipolar fluids at planar interfaces, *Mol. Phys.* 113 (2015) 3750–3756.
- [5] J. M. Prausnitz, R. N. Lichtenthaler, E. Gomes de Azevedo, *Molecular Thermodynamics of Fluid-Phase Equilibria*, Prentice Hall, Upper Saddle River, NJ, USA, 1998.
- [6] R. L. Rowley, W. V. Wilding, J. L. Oscarson, Y. Yang, N. A. Zundel, T. E. Daubert, R. P. Danner, *DIPPR Information and Data Evaluation Manager for the Design Institute for Physical Properties*, AIChE, 2013, Version 7.0.0.

*Corresponding author. E-mail: martin.horsch@mv.uni-kl.de; phone: +49 631 205 3227; fax: +49 631 205 3835.

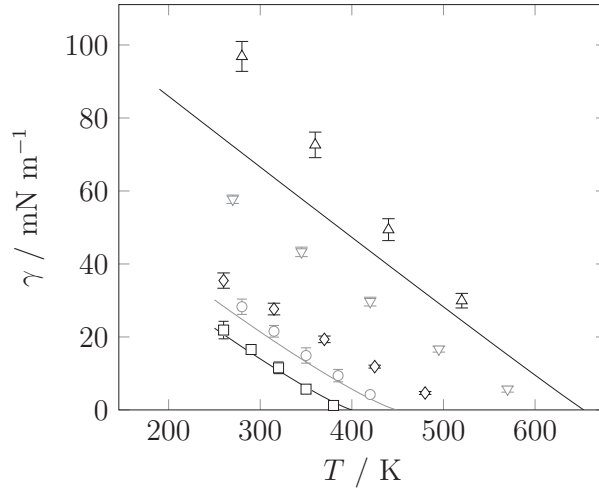


Figure 5: Surface tension as a function of the temperature. Solid lines represent DIPPR correlations to experimental data [6], and symbols are the present simulation results: Hydrazine (Δ), methylhydrazine (∇), 1,1-dimethylhydrazine (\diamond), cyanogen chloride (\circ), and cyanogen (\square). No experimental data are available for methylhydrazine and 1,1-dimethylhydrazine.

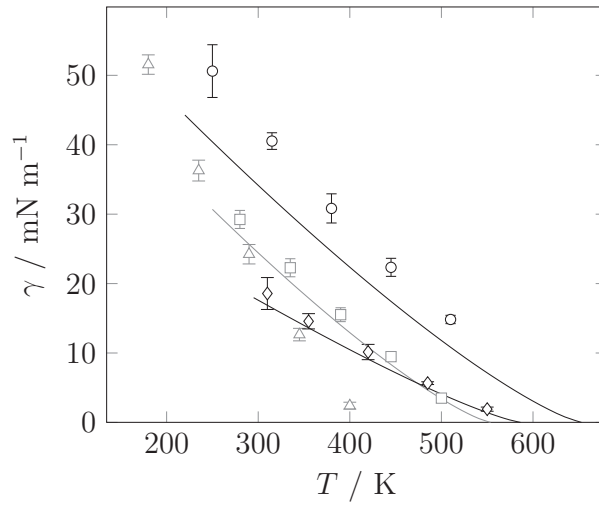


Figure 6: Surface tension as a function of the temperature. Solid lines represent DIPPR correlations to experimental data [6], and symbols are the present simulation results: Cyclohexanone (\circ), cyclohexane (\square), formaldehyde (Δ), and octamethylcyclotetrasiloxane (\diamond). No experimental data are available for formaldehyde.

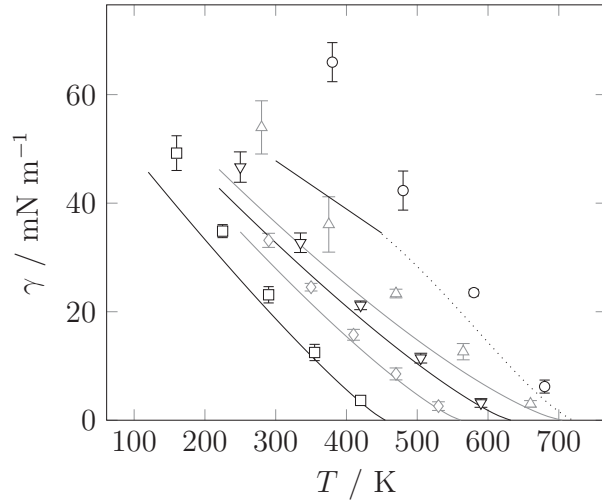


Figure 7: Surface tension as a function of the temperature. Solid lines represent DIPPR correlations to experimental data [6], the dotted line connects the DIPPR correlation with the critical point of ethylene glycol, and symbols are the present simulation results: Ethylene glycol (\circ), ortho-dichlorobenzene (Δ), chlorobenzene (∇), benzene (\diamond), and phosgene (\square).

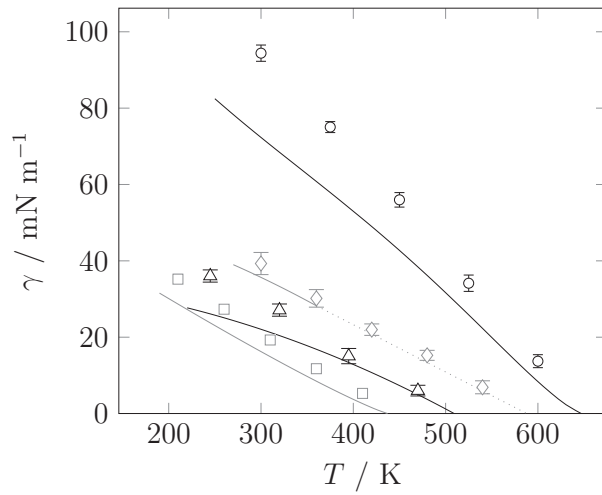


Figure 8: Surface tension as a function of the temperature. Solid lines represent DIPPR correlations to experimental data [6], the dotted line connects the DIPPR correlation with the critical point of formic acid, and symbols are the present simulation results: Water (\circ), formic acid (\diamond), methanol (Δ), and dimethylamine (\square).

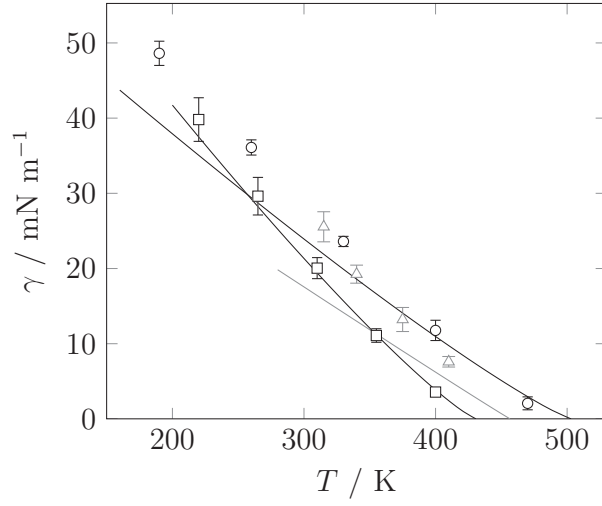


Figure 9: Surface tension as a function of the temperature. Solid lines represent DIPPR correlations to experimental data [6], and symbols are the present simulation results: Dimethyl sulfide (\circ), hydrogen cyanide (\triangle), and sulfur dioxide (\square).

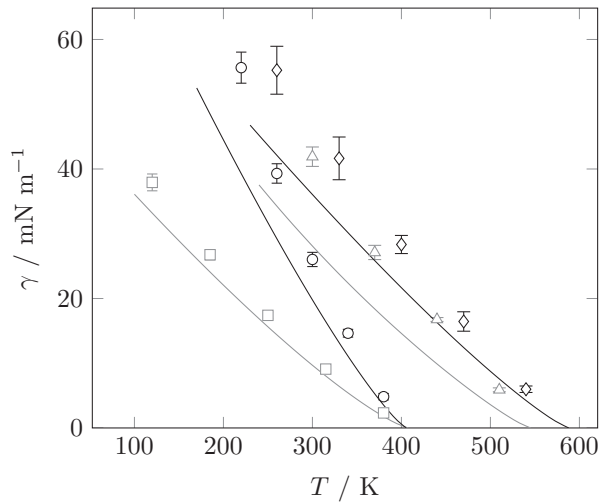


Figure 10: Surface tension as a function of the temperature. Solid lines represent DIPPR correlations to experimental data [6], and symbols are the present simulation results: Nitromethane (\diamond), acetonitrile (\triangle), ammonia (\circ), and isobutane (\square).